The depolymerase activity of MCAK shows graded response to Aurora B kinase phosphorylation through allosteric regulation

The depolymerase activity of MCAK shows graded response to Aurora B kinase phosphorylation through allosteric regulation

Toni McHugh*[1], Juan Zou*[1], Vladimir A. Volkov[2], Aurélie Bertin[4,5], Juri Rappsilber[1,3], Marileen Dogterom[2], Julie P.I. Welburn [1,6]

[1]Wellcome Trust Centre for Cell Biology, School of Biological Sciences, University of Edinburgh, Edinburgh EH9 3BF, Scotland, UK
[2]Department of Bionanoscience, Faculty of Applied Sciences, Delft University of Technology, Delft, Netherlands
[3]Chair of Bioanalytics, Institute of Biotechnology, Technische Universität Berlin, Berlin, German
[4]Laboratoire Physico Chimie Curie, Institut Curie, PSL Research University, CNRS UMR168. 75005 Paris. France
[5]Sorbonne Universités, UPMC University Paris 06, 75005 Paris, France

[6] Corresponding author:
E-mail: Julie.Welburn@ed.ac.uk

*These authors contributed equally to the work

Keywords: MCAK, Aurora B, microtubules, phosphorylation

JCS Advance Online Article. Posted on 21 December 2018

Kinesin-13 MCAK has a compact conformation in solution but is extended on microtubules. Aurora B kinase phosphorylation of MCAK provides graded inhibition of depolymerase activity by disrupting its extended conformation.

Abstract

Kinesin-13 motors regulate precise microtubule dynamics and limit microtubule length throughout metazoans by depolymerizing microtubule ends. Recently, MCAK has been proposed to undergo large conformational changes during its catalytic cycle, as it switches from solution to bound state. Here, we reveal that MCAK has a compact conformation in solution using crosslinking and electron microscopy. When MCAK is bound to the microtubule ends, it adopts an extended conformation with the N terminus and neck region of MCAK interacting with the microtubule. Interestingly, the region of MCAK that interacts with the microtubule is the region phosphorylated by Aurora B and contains an EB-binding motif. The level of phosphorylation of the N terminus results in a graded microtubule depolymerase activity. Here we show the N terminus of MCAK forms a platform to integrate Aurora B kinase downstream signals and in response fine-tunes its depolymerase activity during mitosis. We propose that this allosteric control mechanism allows decoupling of the N terminus from the motor domain of MCAK to allow MCAK depolymerase activity at kinetochores.

Introduction

Regulation of microtubule length is key throughout eukaryotes. Notably, the Kinesin-13 family members are potent microtubule depolymerases, which destabilize microtubule ends to promote catastrophe (Walczak et al., 2013). Kinesin-13 members play a critical role during mitosis to achieve correct spindle assembly and positioning, accurate kinetochore-microtubule attachments and to prevent genomic instability. The tight regulation of microtubule depolymerases is critical to control microtubule length spatially and temporally.

The most potent Kinesin-13 depolymerase is Kif2c, also termed MCAK. The activity of MCAK is inhibited by Aurora B kinase, through phosphorylation on multiple amino acids within its N terminus (Andrews et al., 2004; Lan et al., 2004). These sites are adjacent to the “SXIP”, End-binding (EB)-binding motif and the neck linker region. EB binds MCAK and recruits it to microtubule plus ends (Mennella et al., 2005; Montenegro Gouveia et al., 2010; Moore et al., 2005). Phosphorylation of residues close to the EB-binding motif prevents MCAK association with EBs and subsequent MCAK recruitment to the plus ends of microtubules (Honnappa et al., 2009; Moore et al., 2005). Aurora B kinase phosphorylation of the N terminus of MCAK also inhibits its microtubule depolymerase activity *in vitro* in the absence of EBs (Lan et al., 2004), although the mechanism is unclear. Paradoxically, the recruitment of MCAK to centromere-tethered Sgo2, where MCAK controls inter-kinetochore stretching and chromosome alignment, requires Aurora B kinase activity (Huang et al., 2007; Rattani et al., 2013; Tanno et al., 2010). Thus Aurora B kinase may play a role in fine-tuning the depolymerase activity of MCAK at centromeres rather than fully inhibiting MCAK.

Most *in vitro* studies on the mechanism of MCAK focus on the monomeric motor domain of MCAK. However, full-length MCAK acts as a dimer *in vivo* (Maney et al., 2001). To understand how MCAK destabilizes microtubules in mitosis, it is critical to examine how full-length MCAK interacts with the microtubule and how Aurora B phosphorylation controls the intrinsic activity of MCAK at the molecular level. However, the structure of full-length MCAK and the

molecular mechanism for MCAK regulation remains unclear. To gain insights into the structure of full-length MCAK and its regulation by phosphorylation, we have used biochemistry and cross-linking/mass spectrometry. We demonstrate that full-length MCAK has a compact conformation in solution and becomes extended when bound to microtubules. Aurora B phosphorylation interferes with the extended conformation of MCAK on microtubules. Overall we show that rather than just inhibiting it, Aurora B fine-tunes the activity of MCAK activity to provide graded levels of microtubule depolymerase activity in the cell.

Results and discussion

Full-length dimeric MCAK has a compact structure in solution

Early studies using rotary shadowing electron microscopy (EM) on the kinesin-13 Kif2a showed Kinesin-13s have a globular structure in solution (Noda et al., 1995). Given the high sequence conservation between Kif2a and MCAK, we hypothesized that MCAK would also form a compact structure in solution. To test whether long-range interactions stabilize full-length MCAK to form a compact motor, we analyzed the 3D structure of human MCAK in solution using cross-linking and mass spectrometry. We first used the zero-length cross-linker EDC/NHS on MCAK and obtained no cross-links. However using the BS3 cross-linker, we were able to successfully cross-link MCAK (Fig S1A). We isolated a species with a high-molecular weight of 160 kDa, corresponding to dimeric MCAK from a denaturing gel (Fig S1A). We then analyzed the cross-linked peptides and identified 160 cross-links (Fig S1B, C). To validate them, we examined whether the cross-links obtained within the motor domain were compatible with the crystal structure of the MCAK motor domain (PDB: 2HEH). The majority of cross-links obtained correspond to lysines within 27 Å of each other in the MCAK motor domain, corresponding to the maximum length of BS3 (Fig 1A, B). A few cross-links identified could be due to the dimeric arrangement of MCAK in the presence of the C terminus (Talapatra et al., 2015). Overall, our

data confirmed that the 3D cross-linking/mass spectrometry was highly specific for the native conformation of MCAK in solution.

We next examined the cross-links present in MCAK between the motor and non-motor regions. MCAK is dimeric thus it is not possible to distinguish whether the cross-links are intermolecular or intramolecular. We found the MCAK N terminus cross-links with the C terminus (Fig 1C, Fig S1C). We also identified cross-links between the N and C termini of MCAK and the motor domain suggesting the non-motor regions sample conformations where they are in close proximity to the motor domain. In particular, we observed multiple cross-links between the far C terminus of dimeric MCAK and the motor domain, indicating that the C terminus of MCAK is in close proximity with its motor domain in the context of full-length MCAK (Fig 1C). These data further support the model that the C terminus of MCAK binds to the N terminus and motor domain in solution (Maney et al., 2001; Moore et al., 2005; Talapatra et al., 2015; Zong et al., 2016). Interestingly, the MCAK C terminus cross-linked with residues in a region that encompasses the α4 helix and L12 loop (522-541), which contribute towards the switch II region and the microtubule-binding site. This is in good agreement with the fact that the C terminus of MCAK and the microtubule compete for the microtubule-binding site of MCAK (Talapatra et al., 2015). Overall, this crosslinking approach does not allow us to dissect the contribution of each monomer to the dimeric MCAK organization but point to a compact conformation of MCAK, where the N and C termini of MCAK interact with the motor domain and with each other extensively in solution to form a compact dimer, unlike more extended conventional kinesins.

To gain further insights into the structure of full-length MCAK, we examined full-length dimeric MCAK using negative stain EM (Fig 1D, E). We observed that MCAK has a compact structure, similar to that of Kif2a (Hirokawa, 1998). We then performed 2D class averages of MCAK and GFP-tagged MCAK. A set of representative classes obtained after two successive rounds of 2D alignment and classification are displayed in Figure 1F. U-shaped structures or

opened rings are obtained, corresponding to different views of the protein. The U-shaped view is 9.5 nm long and 5.5 nm wide. The visualized rings are about 9.5 nm in diameter. The folding and compactness of MCAK is not impaired by the presence of a GFP tag at its C terminus. By comparison with a similar analysis performed on MCAK deprived of GFP, we cannot detect any significant difference, implying that the GFP tag might be mobile and not visualized in the classes. Although we could not define the motor domain positions in the class averages, we can conclude that full-length MCAK has a compact conformation in solution.

Aurora B phosphorylation modestly affects MCAK conformation in solution

Aurora B phosphorylates the N terminus of MCAK to reduce its activity and disrupts its interaction with EB proteins (Andrews et al., 2004; Honnappa et al., 2009; Knowlton et al., 2006; Ohi et al., 2004) (Fig S1D). We next examined whether Aurora B phosphorylation of MCAK induces conformational changes that could inhibit MCAK. We generated an Aurora B phosphomimetic MCAK mutant, $MCAK_{S6E}$ to ensure the sample was fully modified on the residues that are phosphorylated *in vivo.* We mutated residues Ser95, Ser109, Ser111, Ser115, Ser166 and Ser192 to glutamate to mimic constitutive phosphorylation. Using quantitative mass spectrometry, we did not find unique cross-links belonging to either MCAK or $MCAK_{S6E.}$ 130 common cross-links in both MCAK and $MCAK_{S6E}$ have peak intensity ratios of MCAK/$MCAK_{S6E}$ 1.77-0.30 (Fig S1E), indicating they have a similar conformation in solution. The cross-links with significant intensity ratios changes are listed in Table 1 (*t*-test, $p<0.05$). The cross-link pairs containing peptide $_{100}$IPAPKESLR$_{108}$, had significantly decreased intensity in $MCAK_{S6E}$ compared to MCAK. This peptide is in the region phosphorylated by Aurora B and makes cross-links with both the motor domain and C terminus (Fig S1D). Thus our data support that Aurora B phosphorylation of the MCAK N terminus slightly opens the compact conformation of MCAK and diminishes the N terminus-motor and C terminus interaction, as previously reported using FRET

(Ems-McClung et al., 2013). However Aurora B phosphorylation of the MCAK N terminus does not induce any major changes in the compact conformation of MCAK in solution.

The N terminus of MCAK interacts with the microtubule

To further examine how Aurora B might affect the interaction between the microtubule and MCAK to inhibit MCAK, we mapped the regions of MCAK that are proximal to microtubule ends. To generate a MCAK:microtubule complex, that would mimic MCAK conformation at microtubule ends, we incubated MCAK with AMP-PNP in the presence of taxol-stabilized microtubules (Andrews et al., 2004; Lan et al., 2004; Zhang et al., 2008) (Fig 2A, B). We used the EDC/NHS cross-linker to identify the amino acids involved in the MCAK:microtubule interaction (Fig 2C). Cross-links were detected between MCAK and the surface of α- and β-tubulin (Fig 2D). We found that residues 415, 418 and 542 in the β5 sheet (close to loop L8) and loop L12 cross-link with β-tubulin, indicating they are close to the microtubule core. Our cross-linking data confirm that MCAK binds to the microtubule core directly, rather than the acidic tail of tubulin. Surprisingly, we also observed multiple cross-links between the N terminus of MCAK and the microtubule. Residues Lys92, Lys99 Lys104 and Ser106, close to the EB-binding motif and the Aurora B phosphorylation sites cross-linked to Glu113, Asp414, Glu423 and Asp424 in α-tubulin. These residues and Lys209 in the neck linker region of MCAK also cross-linked to the acidic patches contributed by Glu108, Glu111, Asp114, Glu157, Glu158 and Asp161 in β-tubulin. Using our cross-linking data and crystal structures of MCAK, kinesin-1 and stathmin bound to 2 tubulin dimers (mimicking microtubules), we could generate a molecular model of MCAK motor:microtubule (Fig 2E) (Gigant et al., 2013; Prota et al., 2013). The MCAK motor binds across a tubulin dimer, leaving space for the N terminus to bind to the longitudinally adjacent tubulin dimer. Our data demonstrate that MCAK adopts an extended conformation when bound to the microtubule and interacts with the microtubule along two tubulin dimers through both its motor domain and its N terminus.

Aurora B kinase gradually reduces the affinity and activity of MCAK for microtubules

The N terminus and the neck of MCAK, which interact with the microtubule lattice, are phosphorylated on multiple residues by Aurora B to inhibit MCAK activity (Andrews et al., 2004; Lan et al., 2004). Interestingly, these sites lie outside of the motor domain, that is the primary microtubule binding region and has depolymerase activity. To define how Aurora B mechanistically reduces MCAK activity, we used MCAK-GFP, MCAK$_{S2E}$-GFP mutated in the neck region on Ser192 and Ser166, and MCAK$_{S6E}$-GFP, mutated both in the neck and N terminus. To determine the residency time and affinity of MCAK for microtubules, we imaged single molecules of MCAK-GFP on microtubules in 80mM K-PIPES (Fig 3A-C). We found that both MCAK-GFP and MCAK$_{S2E}$-GFP could be observed on the lattice. MCAK-GFP had a slightly longer residency time than MCAK$_{S2E}$-GFP (Fig 3A, C). MCAK$_{S6E}$-GFP could barely be observed on microtubules, only remaining bound for a very short amount of time (Fig 3B, C).

To confirm that Aurora B phosphorylation affects the ability of MCAK to bind to microtubules, we phosphorylated MCAK-GFP *in vitro* with Aurora B kinase and imaged it on microtubules (Fig 3B). Similarly to MCAK$_{S6E}$-GFP, Aurora-phosphorylated MCAK very rarely bound to the microtubule and only for very short times, resulting in reduced microtubule residency (Fig 3C, D). At low ionic strength, MCAK mutants and wild-type microtubule association rates were largely comparable (Fig 3D, S2). In 80 mM K-PIPES, MCAK-GFP and MCAK$_{S2E}$-GFP had off-rates of 1.6 ± 0.3 s^{-1} and 3.2 ± 0.3 s^{-1}respectively, while the off-rates for MCAK$_{S6E}$-GFP and Aurora B-phopshorylated MCAK-GFP were significantly and comparably increased to 25.8 ± 2.5 s^{-1}, and 23.4 ± 7.6 s^{-1} respectively (Fig 3D). Phosphomimetic mutations in MCAK and Aurora B-phosphorylation of MCAK increased the MCAK off-rates from the microtubules to the same extent in different ionic conditions (Fig 3D, Fig S2), indicating that the phosphomimetic mutant recapitulates Aurora B-phosphorylated MCAK *in vitro*.

Thus Aurora B phosphorylates the neck and N terminus of MCAK to reduce the affinity of MCAK for microtubules.

To test the implications of Aurora B dependent-phosphorylation of the N terminus and neck of MCAK, we analyzed the microtubule depolymerization activity of MCAK-, MCAK$_{S2E}$- and MCAK$_{S6E}$-GFP. Using a TIRF microscopy-based assay, we incubated MCAK-GFP in the presence of rhodamine-labelled taxol-stabilized microtubules. We then imaged the rate of microtubule depolymerization for MCAK, MCAK$_{S2E}$ and MCAK$_{S6E}$. 62.5 nM dimeric MCAK-GFP rapidly depolymerized microtubules at a rate of 0.90±0.06 μm min^{-1}. MCAK$_{S2E}$–GFP displayed an intermediate level of depolymerization activity with a rate of 0.37±0.05 μm min^{-1}, while the activity of MCAK$_{S6E}$–GFP was further significantly reduced, with a rate of 0.03±0.01 μm min^{-1} (Fig 3E, F). Aurora B-phosphorylated MCAK at the same concentration depolymerized microtubules at 0.18±0.03 μm min^{-1}. In all cases, depolymerization occurred at both ends of the microtubules (Fig 3F).

In conclusion, using EM and cross-linking, we reveal that MCAK has a compact conformation in solution. Our results are in good agreement with FRET data and confirm the X-ray structure of the C terminus of MCAK bound to its motor domain in solution (Ems-McClung et al., 2013; Talapatra et al., 2015; Zong et al., 2016). In the presence of microtubules, MCAK switches to an extended conformation, where the N terminus, the neck and the motor domain of MCAK engage with the microtubule core, while the C terminus is displaced from the motor (Talapatra et al., 2015). The N terminus of MCAK likely binds a tubulin dimer longitudinally adjacent to that occupied by the motor domain. Recent studies published that the full-length MCAK binds over two tubulin dimers, as does the Drosophila homolog Klp10A and human Kif2A (Benoit et al., 2018; Mulder et al., 2009; Ogawa et al., 2017; Trofimova et al., 2018). No electron density is observed for the MCAK N terminus in the EM class averages, likely due to its largely unstructured properties. The neck linker regions of Klp10A and Kif2a are apparent at the intra-dimer interface of the adjacent tubulin heterodimer (Benoit et al., 2018; Trofimova et al., 2018), in good agreement with our data.

Most work on MCAK points towards the motor domain being the main contributor to the interaction of MCAK with microtubules (Ogawa et al., 2017; Patel et al., 2016; Wang et al., 2017; Wang et al., 2015). Our work reveals that the N terminus of MCAK plays a major role in stabilizing dimeric MCAK on both the microtubule lattice and at microtubule ends prior to ATP hydrolysis. These results are surprising given the neck-motor domain alone (amino acids 181-583) has a microtubule-binding interface and displays robust depolymerase activity (Maney et al., 2001). MCAK is dimeric *in vivo*. Thus one N terminus could bind to EB proteins to track the growing ends of microtubules while the other engages with the microtubule lattice to trigger microtubule catastrophe. Our results indicate the N terminus plays an allosteric role in regulating the motor domain-microtubule interaction or may act to optimally position MCAK within the context of the dimer for catalysis.

During mitosis, Aurora B phosphorylates MCAK to dramatically reduce its depolymerase activity in the vicinity of chromosomes and promote spindle assembly and kinetochore capture. Aurora B act through two mechanisms: first it phosphorylates the MCAK N terminus containing the SXIP motif and prevents EB binding (Honnappa et al., 2009). Second, it phosphorylates MCAK on multiple sites to provide a graded level of microtubule depolymerization activity, by modulating the affinity of MCAK for the microtubule lattice. Even a full Aurora B phosphomimetic mutant retains low microtubule depolymerase activity. This is important because the recruitment of MCAK to the centromere receptor Sgo2 requires Aurora B activity (Huang et al., 2007; Tanno et al., 2010). Centromeric MCAK is phosphorylated to some extent by Aurora B, but still retains modest activity to perform its function (Andrews et al., 2004). At centromeres, MCAK regulates interkinetochore stretch, kinetochore oscillations and error correction of merotelic attachments (Jaqaman et al., 2010; Rattani et al., 2013; Wordeman et al., 2007). The proximity of Aurora B at the centromere may determine the number of sites phosphorylated on MCAK. The extent of MCAK phosphorylation could then provide graded levels of microtubule depolymerase activity depending

upon signals integrated by Aurora B at centromeres, such as kinetochore-microtubule attachment status. However, the depolymerase activity of Aurora B-phosphorylated MCAK remains weak. Another possibility is that when the N terminus of MCAK is bound to its centromeric receptor, the microtubule depolymerase activity of the motor domain is uncoupled from the N terminus. The allosteric regulation of MCAK is then lost and the motor domain acts alone with restored depolymerase activity, which could explain the role of MCAK in error correction at merotelic attachments. Future work should address how centromere-bound MCAK engages with the kinetochore-microtubules to regulate this dynamic interface.

Methods

Cloning, expression and purification of MCAK and Aurora B

MCAK and MCAK-GFP constructs were cloned into pFastBac and expressed in Sf9 insect cells. Site-directed mutagenesis was performed using quickchange mutagenesis kit (Agilent). For Aurora B kinase purification, pEC-K-His-SUMO-SENP2-AuroraB$_{55-34}$ and MCNcs-Spectinomycin-INCENP$_{835-903}$ were co-expressed in presence of 50μg/ml spectinomycin and 50μg/ml kanamycin in BL21 codon+ cells overnight at 18°C. Protein expression and purification was performed as previously described in (Talapatra et al., 2015). Protein phosphorylation *in vitro* was performed as previously described (Welburn et al., 2010).

Microtubule Depolymerisation

Silanised coverslips were prepared as in (Bechstedt et al., 2011) except that in place of treatment with Piranha solution slides were incubated overnight in 12% hydrochloric acid at 50°C. Flow chambers were formed using double sided sticky tape, a silanised coverslip and a microscopy slide. Flow chambers were 7-8 µl in volume.

All experiments were carried out in BRB80 buffer. Anti-β tubulin antibodies (T7816, Sigma Aldrich) at a 1:10 dilution were first introduced to the chamber. The surface was then blocked with 1% pluronic F-127 (Sigma Aldrich) and taxol-stabilized 7% Rhodamine-labeled microtubules (Cytoskeleton) were then bound to the glass surface via the antibodies. The surface was then further blocked with BRB80 buffer containing 1 mg/ml casein (Sigma Aldrich) and 20 µM paclitaxel (Sigma Aldrich). Assay buffer consisted of BRB80 with 1 mM ATP, 0.5 mg/ml casein, 20 µM paclitaxel and an oxygen scavenging system (0.2 mg/ml glucose oxidase, 0.035 mg/ml catalase, 4.5 mg/ml glucose, 140 mM β-mercaptoethanol). Varying concentrations of MCAK, $MCAK_{S2E}$, $MCAK_{S6E}$ and phosphorylated MCAK in assay buffer were introduced to the flow chamber, the chamber was then imaged immediately at 37°C. Imaging was performed on a Zeiss Axio Observer Z1 TIRF microscope using a 100x NA1.46 objective and a Photometrics Evolve Delta EMCCD camera controlled by Zeiss Zen Blue software. Depolymerisation assays were performed for up to 10 minutes at 30 fpm or for $MCAK_{S6E}$ and phosphorylated MCAK and low concentrations of MCAK and $MCAK_{S2E}$ a lower frame rate of 6 fpm was used and imaging was performed for 15 minutes. Kymographs were produced using Image J. Depolymerization rates were measured from these kymographs. Images were stored and vizualized using an OMERO.insight client (OME) (Allan et al, 2012).

Single-molecule TIRF microscopy

Measurement of MCAK residence time on microtubule lattice was performed as described (Volkov et al., 2018). Microtubules were polymerized in MRB80 buffer (80 mM K-Pipes (pH 6.9), 1 mM EGTA and 4 mM $MgCl_2$) containing 50 µM tubulin (8% digoxigenin-labeled, 3.5% labeled with HyLite-647), 1 mM GTP and 20% glycerol. After 20 min at 37°C taxol was added to the final concentration of 25 µM, microtubules were polymerized for 10 min more, sedimented in Airfuge (Beckman) for 3 min at 14 psi, and resuspended in 50 µL MRB80 with 40 µM taxol. Coverslips and slides were cleaned using oxygen plasma for 3 min,

immediately dipped in a solution of Plus-One Repel Silane (Sigma-Aldrich) for 5 min, then sonicated in ethanol and rinsed with water.

Flow chambers were made with silanized slides and coverslips, filled with ~0.2 µM anti-DIG antibody (11333089001, Roche, Switzerland) and passivated with 1% tween-20. Then taxol-stabilized microtubules diluted 1:60 were introduced, unbound material was washed out with MRB80 and MCAK at 5-100 pM was introduced in MRB80 supplemented with 1 mM ATP, 1 mg/ml κ-casein, 40 µM taxol, 4 mM DTT, 0.2 mg/ml catalase, 0.4 mg/ml glucose oxidase and 20 mM glucose. Similarity of the on-rates between MCAK constructs was assayed in the same buffer with reduced ionic strength (32 mM K-Pipes, 0.4 mM EGTA and 1.6 mM $MgCl_2$).

MCAK on microtubule lattice was imaged at 23°C using Nikon Ti-E microscope (Nikon, Japan) equipped with the perfect focus system (Nikon), a Plan Apo 100 × 1.45 NA TIRF oil-immersion objective (Nikon), iLas^2 ring TIRF module (Roper Scientific) and a Evolve 512 EMCCD camera (Roper Scientific, Germany). Images were acquired using MetaMorph 7.8 software (Molecular Devices, San Jose, CA) in stream mode (130 ms per frame at full camera chip, 0.16 µm/pixel). To measure the shorter residence times of $MCAK_{S6E}$ and Aurora B-phosphorylated MCAK in 80 mM K-Pipes, images were binned 8x8 during acquisition, increasing the temporal resolution (to 15 ms per frame), but decreasing spatial resolution (0.86 µm/pixel with an additional 1.5x relay lens).

Kymographs were produced in Fiji (Schindelin et al., 2012) using a reslice operation. Residence times were quantified by measuring the time between the landing and detaching of a single MCAK molecule in the kymograph. Only events longer than 3 consecutive frames were taken into account. Distributions of residence times were fitted with single exponential decay curves (Origin Pro 9.0) with offset fixed to 0. Off-rate was quantified as $1/\tau$. To measure on-rate, the total number of landing events was normalized to total observation time, total microtubule length and MCAK concentration as described (Zaytsev et al., 2015).

Protein cross-linking

The mixing ratio of bis(sulfosuccinimidyl)suberate (BS3,Thermo Fisher Scientific) to complex was determined for MCAK using 5 μg aliquots and using a protein-to-cross-linker ratio (w/w) of 1:1, 1:2, 1:3, 1:4, 1:5, 1:6, 1:7 respectively (Figure S1). As the best condition, we chose the ratio that was sufficient to convert most of MCAK into a dimeric form as judged by SDS-PAGE analysis. 10 μg MCAK was mixed with 20 μg BS3 dissolved in cross-linking buffer (10 mM HEPES pH 7, 200 mM potassium acetate pH 7.6) and incubated on ice for 1 h. The reaction was stopped by adding 2.5 M ammonium bicarbonate for 20 min on ice. For MCAK-microtubule cross-linking, 10 μg microtubules were preactivated using a mixture of EDC (1-ethyl-3-(3-dimethylaminopropyl)carbodiimide hydrochloride) and Sulfo-NHS (N-hydroxysulfosuccinimide, Thermo Fisher Scientific) with w/w ratio (microtubules:EDC:Sulfo-NHS) of 1:1:2.2. 20 minutes later, 10 μg MCAK was added. The mixture was incubated for 1h, before quenching with 2.5 M ammonium bicarbonate for 20 min on ice. The reaction mix was separated on a NuPAGE 4–12% Bis–Tris SDS-PAGE using MES running buffer and NuPAGE LDS Sample buffer (ThermoFisher Scientific). The gel was stained with InstantBlue (Expedeon). Cross-linked samples (red box, Fig 3C) were reduced, alkylated and trypsin digested following standard procedures (Maiolica et al., 2007). Cross-linked peptides were fractionated using SCX-StageTips following the published protocol for linear peptides and desalted using C18 StageTips (Rappsilber et al., 2007).

Mass spectrometry

Peptides were analyzed on LTQ Orbitrap Velos (Thermo Fisher Scientific) coupled with Dionex Ultimate 3000 RSLC nano system. The column was packed into a spray emitter (75-μm inner diameter, 8-μm opening, 250-mm length; New Objectives) that was packed with C18 material (ReproSil-Pur C18-AQ 3 μm; Dr Maisch GmbH, Ammerbuch-Entringen, Germany) using an air pressure pump (Proxeon Biosystems). Mobile phase A consisted of water and 0.1% formic acid.

Mobile phase B consisted of 80% ACN acetonitrile and 0.1% formic acid. Peptides were loaded onto the column with 2% B at 500 nl/min flow rate and eluted at 300 nl/min flow rate with two gradients: linear increase from 2% B to 40% B in 150 minutes; then increase from 40% to 95% B in 11 minutes. The eluted peptides were directly sprayed into the mass spectrometer.

Peptides were analyzed using a high strategy: both MS spectra and MS2 spectra were acquired in the Orbitrap. FTMS spectra were recorded at 100,000 resolutions. The eight highest intensity peaks with a charge state of three or higher were selected in each cycle for iontrap fragmentation. The fragments were produced using CID with 35% normalized collision energy and detected by the Orbitrap at 7500 resolution. Dynamic exclusion was set to 90s and repeat count was 1. The mass spectrometric raw files were processed into peak lists using MaxQuant (version 1.5.3.30)(Cox and Mann, 2008), and cross-linked peptides were matched to spectra using Xi software (version 1.6.683). Search parameters were MS accuracy, 6ppm; MS/MS accuracy, 20ppm; enzyme, trypsin; cross-linker, BS3 (including BS3 modification); Max missed cleavages, 4; fixed modification, carbamidomethylation on cysteine; variable modifications, oxidation on methionine; cross-linkable amino acids, N-terminus, lysine, serine, tyrosine and threonine; fragments, b and y ions with loss of H_2O, NH_3 and CH_3SOH. FDR was estimated using XiFDR on 5% residue level (Fischer and Rappsilber, 2017).

Data are available via ProteomeXchange with identifier PXD008215.

To compare MCAK and $MCAK_{S6E}$ quantitatively, a workflow (Müller et al., 2018) that integrated the MaxQuant (v1.5.3.30)(Cox and Mann, 2008) for spectra pre-processing, Xi (v1.6.743, https://github.com/Rappsilber-Laboratory/XiSearch) for cross-linked peptide identification and Skyline (v4.1.0.11717)(MacLean et al., 2010) for MS1-based quantification was used. 130 unique residue pairs were quantified from 232 and 209 auto-validated unique residue pairs in MCAK and $MCAK_{S6E}$ samples respectively across 6 analyses (3 reaction replica, each reaction has 2 injection replica) using Orbitrap Fusion Lumos (Thermo Fisher Scientific) with a “high/high” acquisition strategy. The peptide separation was carried out on an EASY-Spray column (50 cm × 75 µm i.d., PepMap C_{18}, 2 µm

particles, 100 Å pore size, Thermo Fisher Scientific). Mobile phase A consisted of water and 0.1% v/v formic acid. Mobile phase B consisted of 80% v/v acetonitrile and 0.1% v/v formic acid. Peptides were loaded at a flow rate of 0.3 µl/min and eluted at 0.2 µl/min using a linear gradient going from 2% mobile phase B to 40% mobile phase B over 120 min, followed by a linear increase from 40% to 95% mobile phase B in 11 min. The eluted peptides were directly introduced into the mass spectrometer. MS data were acquired in the data-dependent mode with 3 s acquisition cycle. Precursor spectrum was recorded in the Orbitrap with a resolution of 120,000. The ions with a precursor charge state between 3+ and 8+ were isolated with a window size of 1.6 m/z and fragmented using high-energy collision dissociation (HCD) with collision energy 30. The fragmentation spectra were recorded in the Orbitrap with a resolution of 15,000. Dynamic exclusion was enabled with single repeat count and 60 s exclusion duration. The total peak area of 38 linear peptides has been used for run to run normalization. The peak area of each cross-linked residue pairs were calculated from median value of 6 analyses. The data has been analysis with Perseus (v1.5.1.6) for *t*-test (Tyanova et al., 2016).

Electron microscopy and image processing

Before use, the samples were freed of most aggregates by ultracentrifugation for 5 minutes at 90,000 rpm using a TLA-100 rotor and tabletop ultracentrifuge (Optima, Beckman-coulter). The MCAK samples were diluted from 0.025 to 0.1 $mg.mL^{-1}$ before being adsorbed onto a carbon coated electron microscopy grid and negatively stained using uranyl formate 2%. The samples were examined using a Technai G2 200kV equipped with a TVIPS F416 CMOS camera. Data collection was performed at a magnification of 50,000 with a pixel size of 2.13 Å per pixels and a dose of about 10 electrons per $Å^2$.

Alignment and classification into class averages were performed using the Spider software (Frank et al, 1996). Particles were manually windowed out using Boxer (Eman suite) into 135X135 pixels images. A resulting Spider stack of particles was then normalized against the background. A first step of reference-free

alignment and classification was performed from which a selected set of class averages was chosen as new references for multi-reference alignment and classification. Several rounds of multi-reference alignment and classification were then performed, and new references were selected from the class averages until no further improvement was obtained. For MCAK and MCAK-GFP samples, 1039 and 2800 particles were respectively selected.

Generation of a MCAK:tubulin model

The structures of tubulin:stathmin:TTL, tubulin: MCAK and tubulin:Klp10A were superposed using pymol (PDB: 4IIJ, 5MIO and 6B01 respectively) (Gigant et al., 2013; Tan et al., 2008; Wang et al., 2015).

Acknowledgments

We thank C.Walczak and S.Ems-Clung for discussions, JP Arulanandam for the gift of pEC-K-His-SUMO-SENP2-AuroraB$_{55-34}$ and MCNcs-Spectinomycin-INCENP$_{835-903}$ and Zhuo A. Chen for suggestion of quantitative cross-linking data analysis. J.W. and J.R. are supported by Wellcome Senior Research Fellowships (Grant numbers: 207430 and 103139 respectively). The EM work was supported by Institut Curie, Centre National de la Recherche Scientifique (CNRS). M.D. acknowledges funding from the ERC Synergy Grant MODELCELL (609822). The authors acknowledge the Cell and Tissue Imaging (PICT-IBiSA), Institut Curie, member of ANR France-BioImaging (ANR10-INBS-04).

References

Allan, C., J.M. Burel, J. Moore, C. Blackburn, M. Linkert, S. Loynton, D. Macdonald, W.J. Moore, C. Neves, A. Patterson, et al.. 2012. OMERO: flexible, model-driven data management for experimental biology. Nat. Methods. 9:245–253.

Andrews, P.D., Ovechkina, Y., Morrice, N., Wagenbach, M., Duncan, K., Wordeman, L., and Swedlow, J.R. (2004). Aurora B regulates MCAK at the mitotic centromere. Dev Cell *6*, 253-268.

Bechstedt, S., Wieczorek, M., Noujaim, M., and Brouhard, G.J. (2011). Variations on the single-molecule assay for microtubule-associated proteins and kinesins. Methods Mol Biol *777*, 167-176.

Benoit, M., Asenjo, A.B., and Sosa, H. (2018). Cryo-EM reveals the structural basis of microtubule depolymerization by kinesin-13s. Nat Commun *9*, 1662.
Cox, J., and Mann, M. (2008). MaxQuant enables high peptide identification rates, individualized p.p.b.-range mass accuracies and proteome-wide protein quantification. Nat Biotechnol *26*, 1367-1372.
Ems-McClung, S.C., Hainline, S.G., Devare, J., Zong, H., Cai, S., Carnes, S.K., Shaw, S.L., and Walczak, C.E. (2013). Aurora B Inhibits MCAK Activity through a Phosphoconformational Switch that Reduces Microtubule Association. Curr Biol *23*, 2491-2499.
Ems-McClung, S.C., and Walczak, C.E. (2010). Kinesin-13s in mitosis: Key players in the spatial and temporal organization of spindle microtubules. Semin Cell Dev Biol.
Fischer, L., and Rappsilber, J. (2017). Quirks of Error Estimation in Cross-Linking/Mass Spectrometry. Anal Chem *89*, 3829-3833.
Frank J, Radermacher M, Penczek P, Zhu J, Li Y, Ladjadj M, and Leith A. (1996). SPIDER and Web: Processing and Visualization of Images in 3D Electron Microscopy and Related Fields J. Structural Biol. 116: 190-199.
Gigant, B., Wang, W., Dreier, B., Jiang, Q., Pecqueur, L., Pluckthun, A., Wang, C., and Knossow, M. (2013). Structure of a kinesin-tubulin complex and implications for kinesin motility. Nat Struct Mol Biol *20*, 1001-1007.
Hirokawa, N. (1998). Kinesin and dynein superfamily proteins and the mechanism of organelle transport. Science *279*, 519-526.
Honnappa, S., Gouveia, S.M., Weisbrich, A., Damberger, F.F., Bhavesh, N.S., Jawhari, H., Grigoriev, I., van Rijssel, F.J., Buey, R.M., Lawera, A.*, et al.* (2009). An EB1-binding motif acts as a microtubule tip localization signal. Cell *138*, 366-376.
Huang, H., Feng, J., Famulski, J., Rattner, J.B., Liu, S.T., Kao, G.D., Muschel, R., Chan, G.K., and Yen, T.J. (2007). Tripin/hSgo2 recruits MCAK to the inner centromere to correct defective kinetochore attachments. J Cell Biol *177*, 413-424.
Jaqaman, K., King, E.M., Amaro, A.C., Winter, J.R., Dorn, J.F., Elliott, H.L., McHedlishvili, N., McClelland, S.E., Porter, I.M., Posch, M.*, et al.* (2010).

Kinetochore alignment within the metaphase plate is regulated by centromere stiffness and microtubule depolymerases. J Cell Biol *188*, 665-679.
Knowlton, A.L., Lan, W., and Stukenberg, P.T. (2006). Aurora B is enriched at merotelic attachment sites, where it regulates MCAK. Curr Biol *16*, 1705-1710.
Lan, W., Zhang, X., Kline-Smith, S.L., Rosasco, S.E., Barrett-Wilt, G.A., Shabanowitz, J., Hunt, D.F., Walczak, C.E., and Stukenberg, P.T. (2004). Aurora B phosphorylates centromeric MCAK and regulates its localization and microtubule depolymerization activity. Curr Biol *14*, 273-286.
MacLean, B., Tomazela, D.M., Shulman, N., Chambers, M., Finney, G.L., Frewen, B., Kern, R., Tabb, D.L., Liebler, D.C., and MacCoss, M.J. (2010). Skyline: an open source document editor for creating and analyzing targeted proteomics experiments. Bioinformatics *26*, 966-968.
Maiolica, A., Cittaro, D., Borsotti, D., Sennels, L., Ciferri, C., Tarricone, C., Musacchio, A., and Rappsilber, J. (2007). Structural analysis of multiprotein complexes by cross-linking, mass spectrometry, and database searching. Mol Cell Proteomics *6*, 2200-2211.
Maney, T., Wagenbach, M., and Wordeman, L. (2001). Molecular dissection of the microtubule depolymerizing activity of mitotic centromere-associated kinesin. J Biol Chem *276*, 34753-34758.
Mennella, V., Rogers, G.C., Rogers, S.L., Buster, D.W., Vale, R.D., and Sharp, D.J. (2005). Functionally distinct kinesin-13 family members cooperate to regulate microtubule dynamics during interphase. Nat Cell Biol *7*, 235-245.
Montenegro Gouveia, S., Leslie, K., Kapitein, L.C., Buey, R.M., Grigoriev, I., Wagenbach, M., Smal, I., Meijering, E., Hoogenraad, C.C., Wordeman, L.*, et al.* (2010). In vitro reconstitution of the functional interplay between MCAK and EB3 at microtubule plus ends. Curr Biol *20*, 1717-1722.
Moore, A.T., Rankin, K.E., von Dassow, G., Peris, L., Wagenbach, M., Ovechkina, Y., Andrieux, A., Job, D., and Wordeman, L. (2005). MCAK associates with the tips of polymerizing microtubules. J Cell Biol *169*, 391-397.
Mulder, A.M., Glavis-Bloom, A., Moores, C.A., Wagenbach, M., Carragher, B., Wordeman, L., and Milligan, R.A. (2009). A new model for binding of kinesin 13 to curved microtubule protofilaments. J Cell Biol *185*, 51-57.
Müller, F., Fischer, L., Chen, Z.A., Auchynnikava, T., and Rappsilber, J. (2018). On the Reproducibility of Label-Free Quantitative Cross-Linking/Mass Spectrometry. J Am Soc Mass Spectrom *29*, 405-412.
Noda, Y., Sato-Yoshitake, R., Kondo, S., Nangaku, M., and Hirokawa, N. (1995). KIF2 is a new microtubule-based anterograde motor that transports membranous organelles distinct from those carried by kinesin heavy chain or KIF3A/B. J Cell Biol *129*, 157-167.
Ogawa, T., Saijo, S., Shimizu, N., Jiang, X., and Hirokawa, N. (2017). Mechanism of Catalytic Microtubule Depolymerization via KIF2-Tubulin Transitional Conformation. Cell Rep *20*, 2626-2638.
Ohi, R., Sapra, T., Howard, J., and Mitchison, T.J. (2004). Differentiation of cytoplasmic and meiotic spindle assembly MCAK functions by Aurora B-dependent phosphorylation. Mol Biol Cell *15*, 2895-2906.

Patel, J.T., Belsham, H.R., Rathbone, A.J., Wickstead, B., Gell, C., and Friel, C.T. (2016). The family-specific alpha4-helix of the kinesin-13, MCAK, is critical to microtubule end recognition. Open Biol *6*.
Prota, A.E., Magiera, M.M., Kuijpers, M., Bargsten, K., Frey, D., Wieser, M., Jaussi, R., Hoogenraad, C.C., Kammerer, R.A., Janke, C.*, et al.* (2013). Structural basis of tubulin tyrosination by tubulin tyrosine ligase. J Cell Biol *200*, 259-270.
Rappsilber, J., Mann, M., and Ishihama, Y. (2007). Protocol for micro-purification, enrichment, pre-fractionation and storage of peptides for proteomics using StageTips. Nat Protoc *2*, 1896-1906.
Rattani, A., Wolna, M., Ploquin, M., Helmhart, W., Morrone, S., Mayer, B., Godwin, J., Xu, W., Stemmann, O., Pendas, A.*, et al.* (2013). Sgol2 provides a regulatory platform that coordinates essential cell cycle processes during meiosis I in oocytes. Elife *2*, e01133.
Schindelin, J., Arganda-Carreras, I., Frise, E., Kaynig, V., Longair, M., Pietzsch, T., Preibisch, S., Rueden, C., Saalfeld, S., Schmid, B.*, et al.* (2012). Fiji: an open-source platform for biological-image analysis. Nat Methods *9*, 676-682.
Talapatra, S.K., Harker, B., and Welburn, J.P. (2015). The C-terminal region of the motor protein MCAK controls its structure and activity through a conformational switch. Elife *4*.
Tan, D., Rice, W.J., and Sosa, H. (2008). Structure of the kinesin13-microtubule ring complex. Structure *16*, 1732-1739.
Tanno, Y., Kitajima, T.S., Honda, T., Ando, Y., Ishiguro, K., and Watanabe, Y. (2010). Phosphorylation of mammalian Sgo2 by Aurora B recruits PP2A and MCAK to centromeres. Genes Dev *24*, 2169-2179.
Trofimova, D., Paydar, M., Zara, A., Talje, L., Kwok, B.H., and Allingham, J.S. (2018). Ternary complex of Kif2A-bound tandem tubulin heterodimers represents a kinesin-13-mediated microtubule depolymerization reaction intermediate. Nat Commun *9*, 2628.
Tyanova, S., Temu, T., Sinitcyn, P., Carlson, A., Hein, M.Y., Geiger, T., Mann, M., and Cox, J. (2016). The Perseus computational platform for comprehensive analysis of (prote)omics data. Nat Methods *13*, 731-740.
Volkov, V.A., Huis In 't Veld, P.J., Dogterom, M., and Musacchio, A. (2018). Multivalency of NDC80 in the outer kinetochore is essential to track shortening microtubules and generate forces. Elife *7*.
Walczak, C.E., Gayek, S., and Ohi, R. (2013). Microtubule-depolymerizing kinesins. Annu Rev Cell Dev Biol *29*, 417-441.
Wang, W., Cantos-Fernandes, S., Lv, Y., Kuerban, H., Ahmad, S., Wang, C., and Gigant, B. (2017). Insight into microtubule disassembly by kinesin-13s from the structure of Kif2C bound to tubulin. Nat Commun *8*, 70.
Wang, W., Shen, T., Guerois, R., Zhang, F., Kuerban, H., Lv, Y., Gigant, B., Knossow, M., and Wang, C. (2015). New Insights into the Coupling between Microtubule Depolymerization and ATP Hydrolysis by Kinesin-13 Protein Kif2C. J Biol Chem *290*, 18721-18731.
Welburn, J.P., Vleugel, M., Liu, D., Yates, J.R., 3rd, Lampson, M.A., Fukagawa, T., and Cheeseman, I.M. (2010). Aurora B phosphorylates spatially distinct

targets to differentially regulate the kinetochore-microtubule interface. Mol Cell *38*, 383-392.
Wordeman, L., Wagenbach, M., and von Dassow, G. (2007). MCAK facilitates chromosome movement by promoting kinetochore microtubule turnover. J Cell Biol *179*, 869-879.
Zaytsev, A.V., Mick, J.E., Maslennikov, E., Nikashin, B., DeLuca, J.G., and Grishchuk, E.L. (2015). Multisite phosphorylation of the NDC80 complex gradually tunes its microtubule-binding affinity. Mol Biol Cell *26*, 1829-1844.
Zhang, L., Shao, H., Huang, Y., Yan, F., Chu, Y., Hou, H., Zhu, M., Fu, C., Aikhionbare, F., Fang, G.*, et al.* (2011). PLK1 phosphorylates mitotic centromere-associated kinesin and promotes its depolymerase activity. J Biol Chem *286*, 3033-3046.
Zhang, X., Ems-McClung, S.C., and Walczak, C.E. (2008). Aurora A phosphorylates MCAK to control ran-dependent spindle bipolarity. Mol Biol Cell *19*, 2752-2765.
Zong, H., Carnes, S.K., Moe, C., Walczak, C.E., and Ems-McClung, S.C. (2016). The far C-terminus of MCAK regulates its conformation and spindle pole focusing. Mol Biol Cell *27*, 1451-1464.

Figures

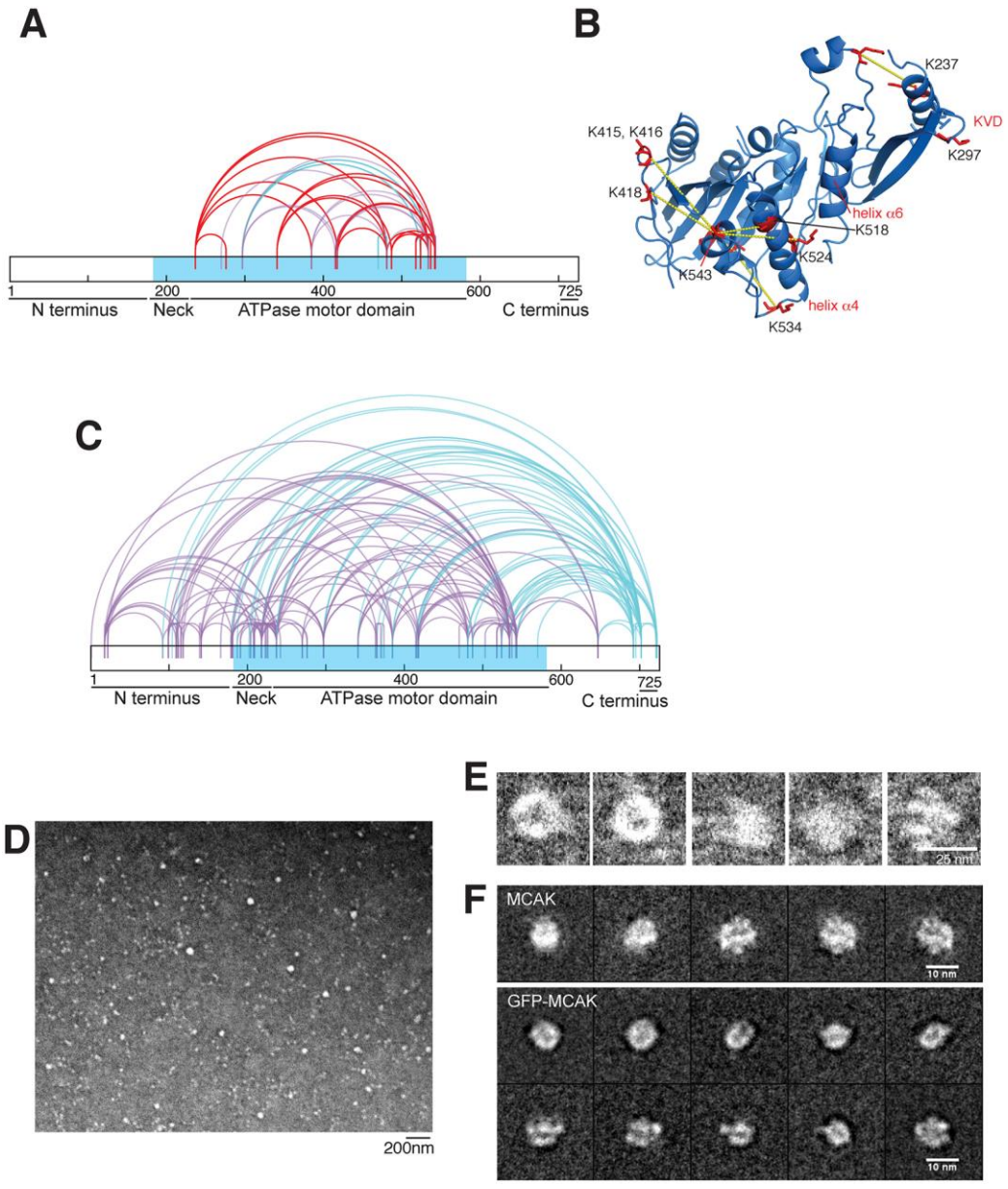

Figure 1: MCAK has a compact conformation in solution. (A) Cross-links for amino-acids in the MCAK motor domain crystal structure (PDB:4UBF, 2HEH) within 27A in the monomer (red), between two monomers in the asymmetric unit (blue) or not present (purple). (B) MCAK motor domain structure (PDB: 2HEH) showing cross-links (dashed lines) and lysine amino acids involved (red). (C)

Cross-linking pattern of full-length MCAK highlighting the motor domain (sky blue) and cross-links involving the far C-terminus (blue). (D) Negative stain EM micrograph of MCAK particles. (E) MCAK particles picked for image analysis and classification. (F) Class averages of negative-stained MCAK and MCAK-GFP.

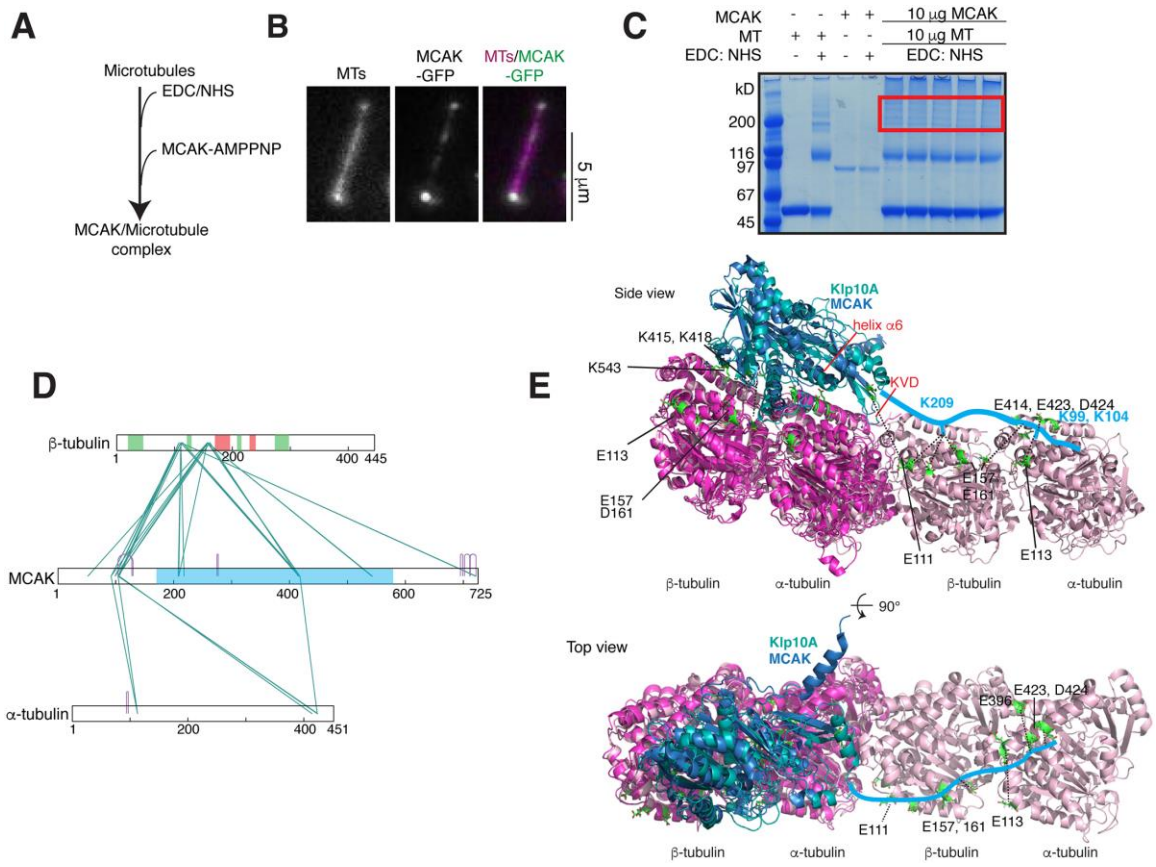

Figure 2: MCAK has an extended conformation on microtubules. (A) Experimental setup for cross-linking MCAK to microtubule ends. Microtubules were pre-activated with EDC/sulfo-NHS, followed by the addition of MCAK and AMPPNP. (B) Representative image of a microtubule bound to MCAK-GFP in the presence of AMPPMP *in vitro*. (C) SDS-PAGE coomassie-stained gel showing MCAK-tubulin cross-linking with EDC/sulfo-NHS. The region selected for trypsin digestion and peptide extraction is boxed in red. (D) Linkage map showing sequence positions of the cross-linked residue pairs between MCAK and porcine α- and β-tubulin. Regions of β-tubulin involved in longitudinal (red) and lateral (green) contacts and the MCAK motor domain (sky blue) are highlighted. (E) Structural model of MCAK and Klp10A binding microtubules in cartoon representation. The MCAK:tubulin crystal structure (blue:magenta, PDB: 5MIO) is overlaid with the cryo-EM structure of Kinesin-13, Klp10A, bound to microtubules (cyan, PDB:6B01). Tubulin dimers from the structure of stathmin:tubulin:TTL are overlaid in pink (PDB: 4IIJ). MCAK:tubulin cross-links are highlighted green in stick representation. The N terminal extension of MCAK is drawn in light blue.

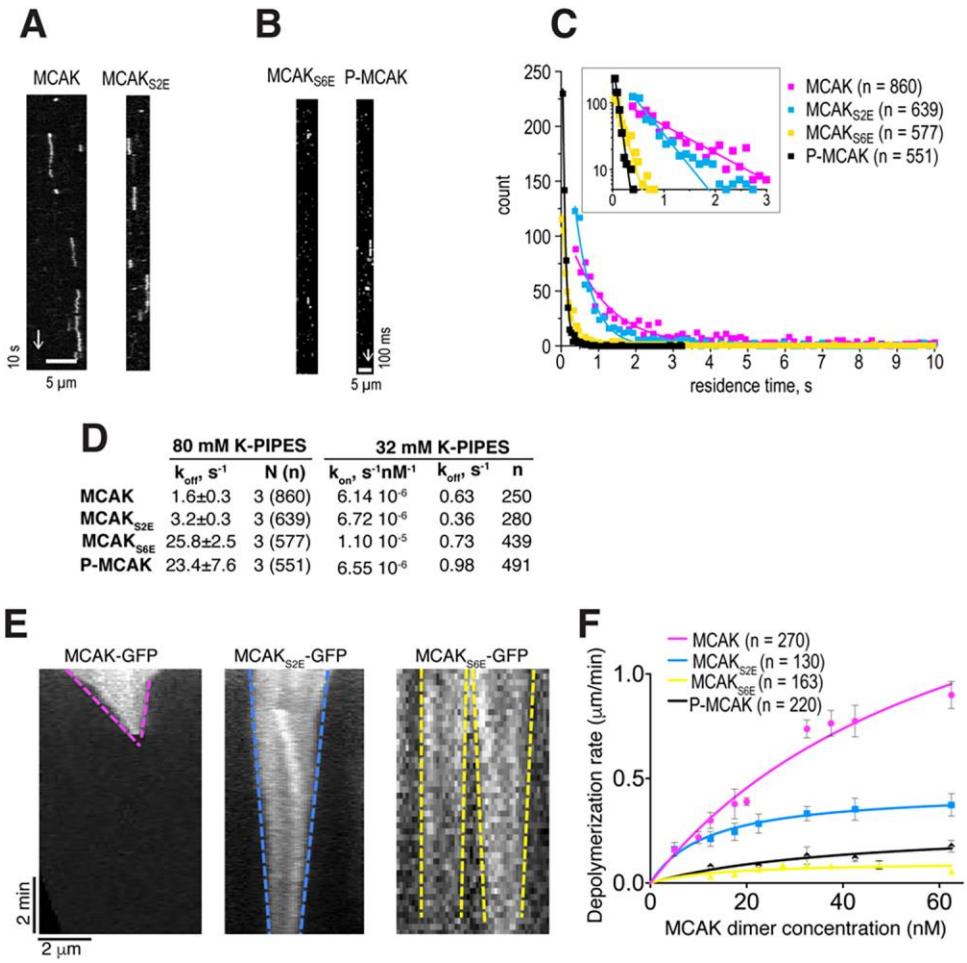

	80 mM K-PIPES		32 mM K-PIPES		
	k_{off}, s^{-1}	N (n)	k_{on}, $s^{-1}nM^{-1}$	k_{off}, s^{-1}	n
MCAK	1.6±0.3	3 (860)	$6.14\ 10^{-6}$	0.63	250
MCAK$_{S2E}$	3.2±0.3	3 (639)	$6.72\ 10^{-6}$	0.36	280
MCAK$_{S6E}$	25.8±2.5	3 (577)	$1.10\ 10^{-5}$	0.73	439
P-MCAK	23.4±7.6	3 (551)	$6.55\ 10^{-6}$	0.98	491

Figure 3: Aurora B inhibits MCAK by gradually increasing its microtubule off-rate. (A) Representative kymographs showing single molecules of MCAK-GFP and MCAK$_{S2E}$-GFP diffusing on stable microtubules in 80mM K-PIPES. (B) Kymographs of binned acquisitions used to quantify residence times of MCAK$_{S6E}$-GFP and phosphorylated MCAK-GFP. (C) Distributions of residence times for MCAK-GFP mutants and Aurora B-phosphorylated MCAK-GFP in 80 mM K-Pipes fitted with single exponential curves. (D) Association and dissociation rates of MCAK-GFP mutants and Aurora B-phosphorylated MCAK-GFP in 80mM and 32mM K-PIPES. (E) Representative kymographs of microtubules depolymerizing in the presence of MCAK-GFP mutants (125nM). (F) Average microtubule depolymerization rates (mean and s.e.) for MCAK-GFP mutants and Aurora B-phosphorylated MCAK-GFP, varying concentrations, fitted with modified Hill equations.

Table 1: Cross-links with statistically significant changes in intensity for MCAK/MCAK$_{S6E}$ ratios.

Cross-link peptide 1	Cross-link peptide 2	Cross-link sequence No	Area	Ratio MCAK/MCAK$_{S6E}$	-Log(p value)*	t-test Difference
DNLPLQENVTIQKQK	GSSSANPVNSVR	90_179	N-term_N-term	0.68	2.85	-4.50E+06
IPAPKESLR	MoxIKEFR	104_237	N-term_Motor	1.26	2.04	1.75E+07
IPAPKESLR	LKVDLTK	104_297	N-term_Motor	1.64	4.16	8.50E+07
IPAPKESLR	DVIKALR	104_702	N-term_C-term	1.44	3.30	1.26E+08
KAQNSEMoxR	LKVDLTK	209_297	Neck_Motor	0.82	2.69	-1.95E+08
AQEYDSSFPNWEFAR	MoxIKEFR	223_237	Neck_Motor	0.84	2.73	-5.31E+07
KRPLNKQELAK	THTMoxGGDLSGK	270_363	Motor_Motor	0.59	2.19	-9.93E+07
ESKLTQVLR	KRPQ	543_722	Motor_C-term	0.81	2.19	-6.09E+07

*p value<0.05 as threshold

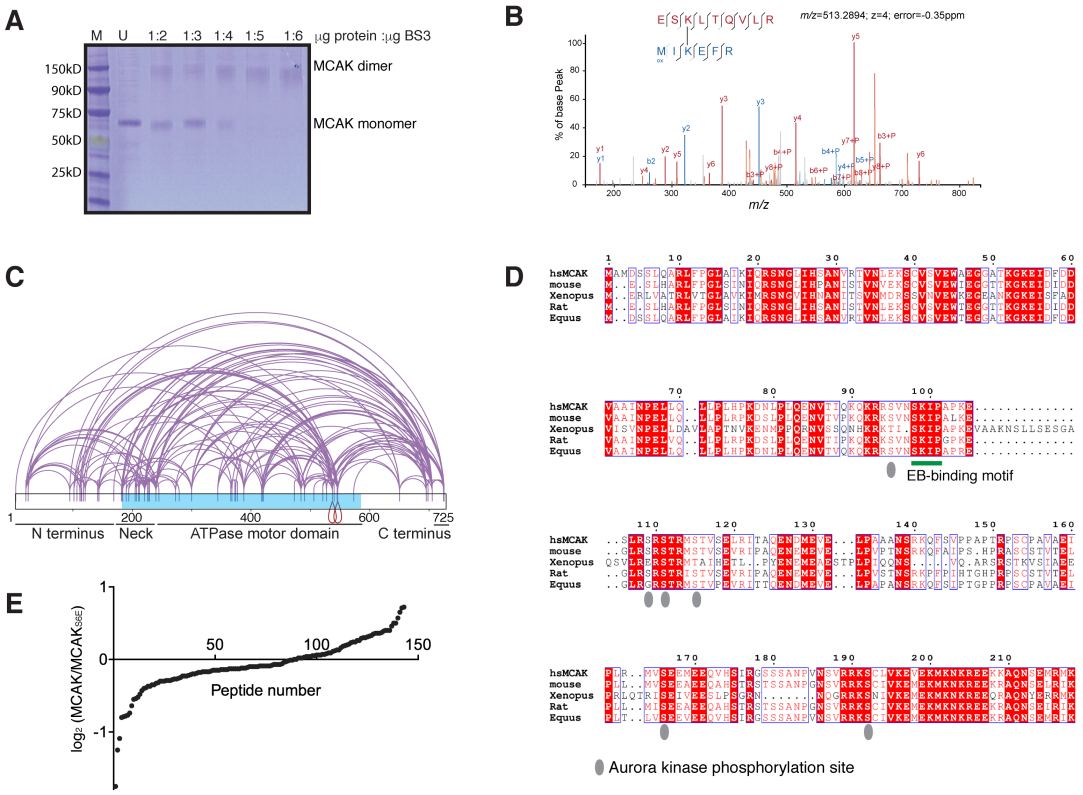

Figure S1. (A) SDS-PAGE coomassie-stained gel showing MCAK cross-linking with increasing amounts of BS3 cross-linker. U: uncross-linked. (B) Fragmentation spectrum of a cross-linked peptide pair that includes a link between Lys543 and Lys237. MS2 peaks supporting peptide sequence $ESK_{543}LTQVLR$ are annotated in red, and those supporting $MIK_{237}EFR$ are annotated in blue. (C) Cross-link pattern of MCAK using 5% FDR cut off. (D) Sequence alignment of MCAK for human, mouse, Xenopus, rat and horse species, highlighting conserved residues in red. Aurora B phosphorylated residues and the EB-binding motif are indicated. (E) Fold change of $\log_2$ ratio for $MCAK/MCAK_{S6E}$ peptides.

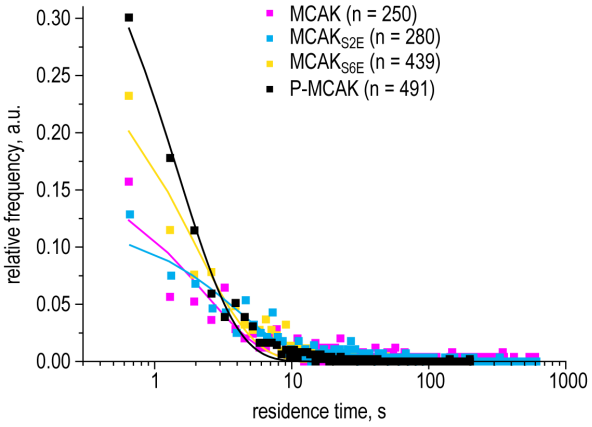

Figure S2. Distributions of residence times for MCAK-GFP (pink), MCAK$_{S2E}$–GFP (blue), MCAK$_{S6E}$-GFP (yellow) and Aurora B-phosphorylated MCAK-GFP (black) in 32 mM K-Pipes fitted with single exponential curves.